




# Role of the plasticizers on the crystallization of PLA and its composites with mesoporous MCM-41

Enrique Blázquez-Blázquez<sup>1,\*</sup>, Rosa Barranco-García<sup>1,2</sup>, Tamara M. Díez-Rodríguez<sup>1</sup>, María L. Cerrada<sup>1,\*</sup> , and Ernesto Pérez<sup>1</sup>

<sup>1</sup> Instituto de Ciencia y Tecnología de Polímeros (ICTP-CSIC), Juan de la Cierva 3, 28006 Madrid, Spain

<sup>2</sup> Departamento de Química Orgánica, Facultad de Ciencias Químicas, Universidad Complutense de Madrid, Avda. Complutense s/n, 28040 Madrid, Spain

**Received:** 3 November 2023

**Accepted:** 1 March 2024

**Published online:**  
21 March 2024

© The Author(s), 2024

## ABSTRACT

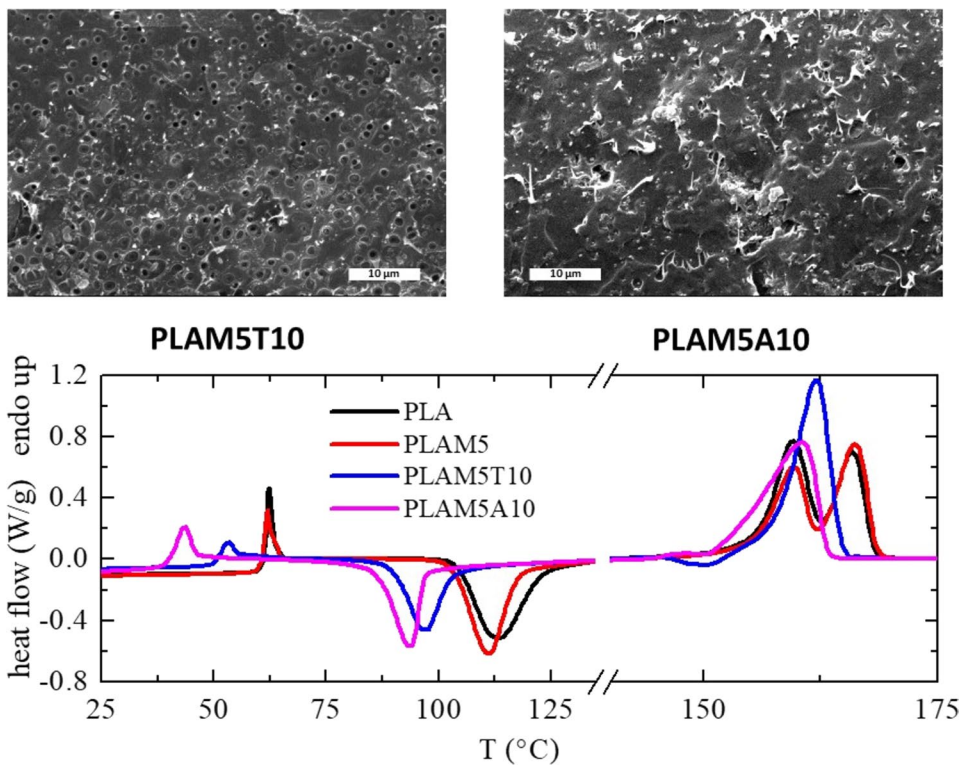
Several materials were prepared by melt extrusion, based on an *L*-rich polylactide (PLA), as polymeric matrix, acetyl tri-*n*-butyl citrate (ATBC) or trioctyl trimellitate (TOTM), as plasticizer, and mesoporous MCM-41 particles, playing a nucleant role. Influence of the addition of these nucleating particles, together with the comparative effect of the two plasticizers, has been thoroughly evaluated on the features of the several phase transitions existing in the PLA polymeric matrix (glass transition, cold crystallization,  $\alpha'$  to  $\alpha$  transition, melting processes and melt crystallization) as well as on the rate of PLA crystallization. The window where this ordering process can take place is shifted down to lower temperatures for these binary and ternary systems and the range of temperatures at which the  $\alpha'$  and  $\alpha$  polymorphs crystallize under isothermal crystallization from the glassy state significantly changes in the materials containing ATBC as plasticizer, either the binary or ternary ones. Type of the major crystalline lattice developed at 85 and 110 °C has been confirmed, additionally to the DSC experiments, by FTIR spectroscopy.

Handling Editor: Gregory Rutledge.

Address correspondence to E-mail: enrique.blazquez@ictp.csic.es; mlcerrada@ictp.csic.es

<https://doi.org/10.1007/s10853-024-09556-x>

## GRAPHICAL ABSTRACT



## Introduction

Poly(lactide) (PLA) is a biobased aliphatic polyester, being also well-known because of its biodegradable and biocompatible character. Its origin from renewable sources along with its noticeable properties makes it suitable for countless applications at present and in the near future. PLA exhibits, however, a rather lessened capacity for crystallization under the regular conditions that are used during the processing of polymers [1] and, in addition, shows a relatively high brittleness. The first aspect is ascribed to its low rate of crystallization, while the second one is associated with the position of its glass transition temperature ( $T_g$ ), which is usually observed at about 60 °C. These two main shortcomings can be solved by incorporation of specific additives. On one hand, incorporation of agents boosting crystallite nucleation turns out an appropriate approach for solving its reduced ability for three-dimensional ordering. And, on the other hand, addition of plasticizers can tune location of  $T_g$ , since these compounds promote the rise of the global mobility within the polymeric macrochains.

All of the nucleating agents or the plasticizers do not have, however, an analogous impact in the final behavior of PLA. As just commented, the function of the former is to change the rate of PLA nucleation by creating a growing number of primary sites that allow a reduction in the induction period of this nucleation stage. Distinct agents have been examined in PLA, including mineral or organic compounds and mineral-organic hybrids [2]. Talc has demonstrated to exert an important influence in the PLA crystallization and, then, it accounted as a reference in the evaluation of capacity of the PLA nucleation promoted by different nucleants [2, 3]. Pristine or functionalized carbon nanotubes have been also used [2], owing to their prominent thermal, mechanical and electrical properties ascribed to their significant aspect ratio. The nucleating role of mesoporous silica in PLA has been recently analyzed as well. Incorporation of SBA-15 particles has turned out very efficient in the crystallization of PLA, as described in extruded composites [4, 5] and in others prepared from solution [6]. Particles of the mesoporous SBA-15 silica exhibit hexagonal arrangements in their interior, which

are developed along the synthetic process. They are constituted by ordered hollow channels, whose diameters range from around 7 to 10 nm [7].

Addition of plasticizers contributes to improve ductility and processability of polymers through the reduction of intra and intermolecular interactions within their macrochains. Accordingly, flexibility is significantly enhanced. This increase in mobility involves the displacement of  $T_g$  to inferior temperatures. This fact turns out very attractive in PLA because, on one hand, the negative effect of physical aging might be minimized whether the decreasing shift of its  $T_g$  is large enough. And, on the other hand, its crystallization window may be simultaneously moved at lower temperatures. A suitable effect of the plasticizer is, however, controlled by several variables: the nature of matrix, the plasticizer type, its thermal stability at temperature of processing, and the selection of an optimal content, among others. Furthermore, presence of plasticizers can also alter different characteristics within the crystalline regions, as crystallite size and, accordingly, the melting temperature ( $T_m$ ). In fact, a depression of  $T_m$  has been described in previous investigations [8, 9]. Several types of plasticizers have been evaluated for PLA, such as glucose monoesters and partial fatty acid esters, bishydroxymethyl malonate (DBM) [10], citrates [11], atactic poly(3-hydroxybutyrate) (a-PHB) [12, 13], poly(ethylene glycol) (PEG) [11, 14, 15], poly(propylene glycol) (PPG) [16], or oligoesteramide (DBM-oligoesteramide) [10, 17, 18], among others. In addition, the choice of plasticizer might be also limited by legislative requirements for some of the PLA applications, such as in the biomedical or in the food packaging fields, resulting the selection even more difficult [10, 18].

Some aspects of the crystallization behavior of composites of PLA with mesoporous Mobile Crystalline Material 41 (MCM-41) using, additionally, the acetyl tri-*n*-butyl citrate (ATBC) as plasticizer have been analyzed in a previous article [19]. The purpose of this work is to extend that investigation to a different plasticizer, the trioctyl trimellitate (TOTM), by evaluating how addition of the ATBC or the TOTM affects the crystallization characteristics exhibited by the pure PLA or by the PLA in composites with MCM-41 silica [20] as nucleant. Furthermore, a heating rate of 120 °C/min, instead of the 60 °C/min employed before [19],

is used in this study. This very high rate allows preventing cold crystallization of the sample during its heating from the glassy state to the isothermal temperature, in order to attempt observation of the PLA crystallization rate throughout its entire crystallization window. The ATBC has been selected for its adequate solubility with PLA, which is a feature shared with other citrate-based plasticizers, as described in literature [1, 9, 18, 21]. On the other hand, TOTM has been chosen for its durability and heat resistance characteristics [22]. Incorporation of mesoporous MCM-41 silica within PLA in the composites allows comparing the single role of each plasticizer on the PLA ordering (either under dynamic or isothermal conditions) in the binary materials and the combined nucleant/plasticizer action (if any) in the ternary systems. This latest will provide an idea on the possible existence of a synergistic influence between both additives: the one reducing the activation energy of nucleation (mesoporous MCM-41) and the plasticizer that increases flexibility of the PLA amorphous phase and displaces its interval of crystallization to lower temperatures. The dual addition of nucleating agent and plasticizer has been explored in literature [23–26] since it can turn out rather successful from practical and scientific standpoints because some of the important drawbacks shown in PLA by either its amorphous or crystalline phases can be simultaneously solved: enthalpic recovery and difficulty for crystallizing, respectively. A content of 10 wt.% in TOTM has been chosen for this study, both without and with MCM-41 silica, based on the results attained in our previous investigation [19] and in order to reach a good compromise between the amount of plasticizer and the effect on the crystallization rate of PLA (and on the actual crystallization window). Accordingly, binary and ternary materials are required for this research. The former incorporate PLA and a suitable amount of plasticizer (either ATBC or TOTM) while the latter are composed by PLA together with a given content of MCM-41 and of plasticizer. A comprehensive study by differential scanning calorimetry (DSC) has been carried out under non-isothermal and isothermal protocols, being analyzed distinct crystallization temperatures using as initial starting points either the molten or the glassy states of PLA, in order to gain a better understanding of the different parameters involved.

## Experimental part

A commercially available polylactide (PLA) from NatureWorks® (labeled as Ingeo™ Biopolymer 6202D, with a density of 1.24 g/cm<sup>3</sup>, and a content in *L*-isomer units of about 98 mol%) is used in this study. Its weight-average molecular weight ( $M_w$ ) and molecular weight dispersity are 118,600 g/mol and 1.6, respectively, as determined from gel permeation chromatography (GPC) [27].

The acetyl tri-*n*-butyl citrate (ATBC) (CAS 77-90-7) plasticizer and the trioctyl trimellitate (TOTM) (CAS 3319-31-1) were purchased from Sigma-Aldrich with purity equal or greater than 98.0%. Their chemical structures are depicted in Scheme 1. ATBC has a molecular weight of 402.5 g/mol and a boiling temperature of 331 °C, while molecular weight for TOTM is 546.8 g/mol and its boiling temperature shows a value of 414 °C.

The MCM-41 particles were purchased also from Sigma-Aldrich (specific surface area,  $S_{BET} = 966 \text{ m}^2/\text{g}$ ; average mesopore diameter,  $D_p = 2.9 \text{ nm}$  [28]) and were used as received.

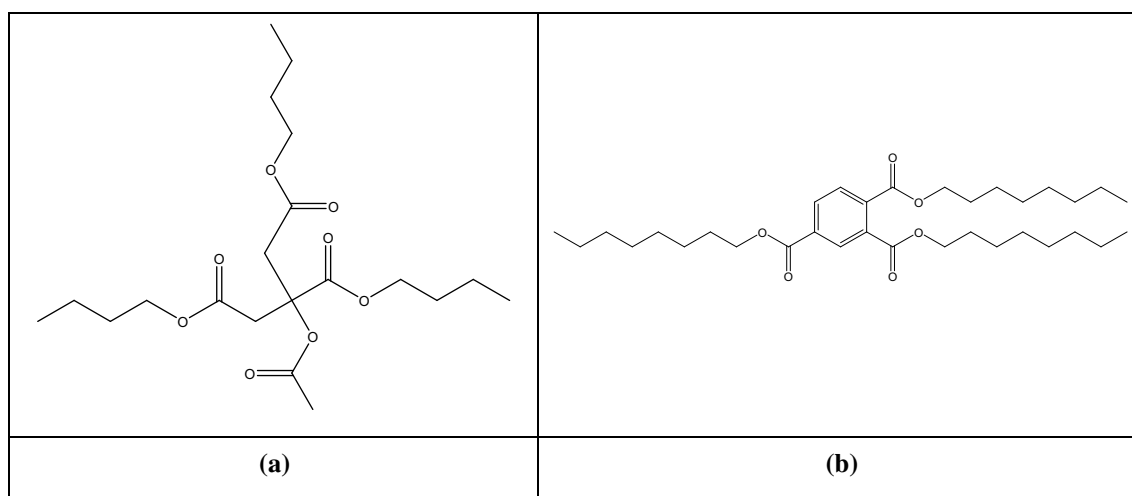
PLA, PLA-ATBC and PLA-TOTM binary blends at a plasticizer content of 10 wt.%, binary composite of PLA and MCM-41 in a weight amount of 5%, along with PLA/ATBC/MCM-41 and PLA/TOTM/MCM-41 ternary composites, at those compositions of plasticizer and MCM-41, were prepared through a melting processing in a micro-conical twin screw Thermo Scientific Haake Minilab miniextruder operating at 190 °C, with a screw speed of 100 rpm,

using a mixing time of 4 min after the full feeding. Designation of samples is detailed in Table 1 according to its actual content in the different constituents as determined by thermogravimetry (see below). PLA and MCM-41 were dried previous extrusion. The former was initially placed in an oven at 85 °C for 20 min followed by a drying under vacuum at 85 °C for 2 h. The MCM-41 silica was dried under vacuum at 100 °C for 24 h.

The extrudates were collected at room temperature as bulk material, and immediately placed under vacuum at 85 °C, and left there for 2 h before processing them by compression molding in a hot-plate Collin press. Initially, the material was maintained at a temperature of 190 °C without pressure for 2 min and, then, a pressure of 25 bar was applied for 5 min. Afterward, and while maintaining the pressure, the different composites were cooled, with recirculating water inside the plates, from their molten state to room

**Table 1** Sample designation and actual content in the different constituents: PLA, MCM-41 silica, and ATBC or TOTM plasticizers, for the different materials

| Sample   | Content (wt.%) |        |      |      |
|----------|----------------|--------|------|------|
|          | PLA            | MCM-41 | ATBC | TOTM |
| PLA      | 100            | 0      | 0    | 0    |
| PLAM5    | 95.3           | 4.7    | 0    | 0    |
| PLAM0A10 | 91.0           | 0      | 9    | 0    |
| PLAM5A10 | 83.7           | 5.3    | 11   | 0    |
| PLAM0T10 | 90.0           | 0      | 0    | 10   |
| PLAM5T10 | 86.1           | 4.9    | 0    | 9    |



**Scheme 1** Chemical structure of the ATBC (a) and TOTM (b) plasticizers

temperature (at a relatively rapid rate of around 80 °C/min). The compressed films were then stored at ambient conditions in sealed plastic bags and left there for around 1 week before proceeding to their characterization. These original compression-molded films were totally amorphous, as shown below from the zero neat enthalpy involved in the first heating DSC curves.

Morphological details of the mesoporous MCM-41 were obtained by transmission electron microscopy (TEM). Measurements were performed at room temperature in a 200 kV JEM-2100 JEOL microscope. The particles were dispersed in acetone in an ultrasonic bath for 5 min and then deposited in a holder prior to observation. Furthermore, experiments of high-resolution field emission scanning electron microscopy (FESEM) were carried out in a S-8000 Hitachi equipment at room temperature on those particles dispersed in acetone and deposited in a holder.

Fracture surface in different sections of the films was evaluated by scanning electron microscopy (SEM) using a Philips XL30 microscope. The samples were coated with a layer of 80:20 Au/Pd alloy and deposited in a holder before visualization.

Thermogravimetric analysis (TGA) was performed in a Q500 equipment of TA Instruments, under air atmosphere at a heating rate of 10 °C/min. The actual amount of these two additives, plasticizer (TOTM or ATBC) and nucleating agent (MCM-41), incorporated into the extruded materials is determined and listed in Table 1 for the different composites.

Calorimetric analyses were carried out in a TA Instruments Q100 calorimeter connected to a cooling system and calibrated with different standards. The sample weights were around 3 mg. A temperature interval from –30 to 190 °C was studied at a heating rate of 10 °C/min in dynamic experiments. Isothermal measurements have been also performed either from the molten or from the glassy state.

Isothermal experiments from the melt were carried out as follows: a rapid cooling, at 60 °C/min, was applied from 190 °C to the desired crystallization temperature,  $T_c$ , which was isothermally maintained for the required time. Subsequently, the heating curve at 10 °C/min is registered. The crystallization temperatures were extended to those values where the crystallization is complete after a reasonable time (total crystallization times requiring longer than around 100 min show already a very bad signal-to-noise ratio).

Details for isothermal experiments from the glassy state are the next: starting again at 190 °C, a rapid cooling is carried out at 60 °C/min, now until below the glass transition of the sample. Then, the desired crystallization temperature is reached by heating at 120 °C/min, being isothermally maintained for the required time. Afterward, the subsequent heating curve is registered at 10 °C/min. The use of this high rate, 120 °C/min, avoids cold crystallization to take place in the sample during its heating up to the isothermal crystallization temperature.

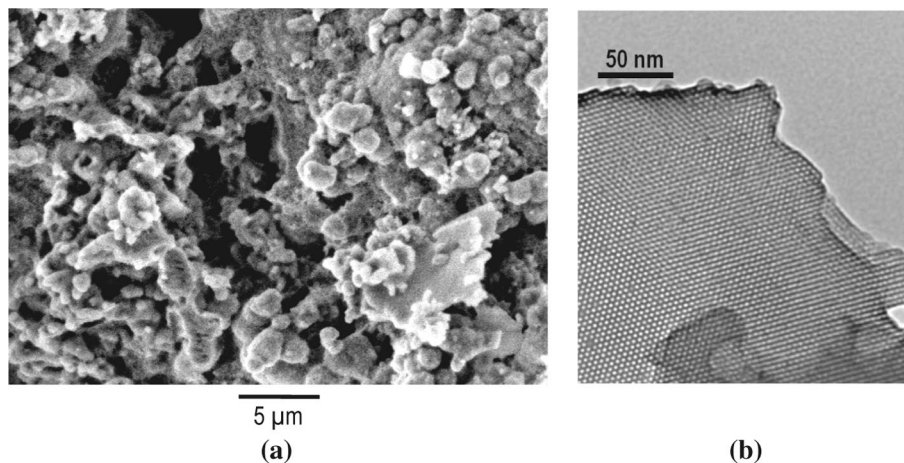
All the DSC curves presented throughout this work are actual curves without normalization for the real content of PLA in the sample. That normalization has been performed, however, for the enthalpies used to estimate crystallinity degree of the different experiments, i.e., the values achieved are then the normalized crystallinity. For the determination of the crystallinity, 93.1 J/g was used as the enthalpy of fusion of a perfectly crystalline material [29, 30].

## Results and discussion

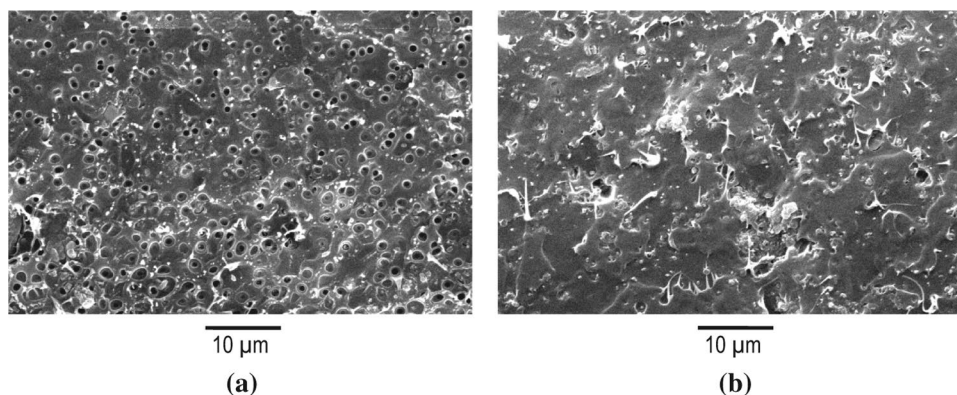
Figure 1a displays the FESEM picture for the neat MCM-41 particles, which was achieved from dispersion of the silica in acetone and their further deposition. These observed aggregates are composed by microsized particles of mesoporous MCM-41, which show a non-regular shape. This result is in agreement with others previously reported in literature [31, 32]. A higher magnification, attained by using TEM, allows observation of the interior of particles, as depicted in the image of Fig. 1b. Existence of ordered arrangements framed in a hexagonal morphology is now revealed. MCM-41 is then composed by a well-defined structure of channels [20], whose diameters are around 3 nm.

Figure 2 shows SEM pictures at the fracture for the ternary composites incorporating TOTM (left) or ATBC (right) as plasticizer in the PLA/MCM-41 materials. A clear difference is noticed when these two samples, PLAM5T10 and PLAM5A10, are compared. Observation of the fracture region in the former shows the existence of numerous voids, while this area is rather continuous in the PLAM5A10 specimen. This fact seems to indicate the distinct solubility existing between PLA and the plasticizer added, being higher in the case of using ATBC, as already described in literature [1, 9, 18, 21], and more deficient for the TOTM, as

**Figure 1** a FESEM and b TEM micrographs of MCM-41 particles dispersed in acetone and further deposited in a holder.



**Figure 2** SEM pictures from the fracture area for the ternary materials: (a) PLAM5T10 and (b) PLAM5A10 composites.



deduced from the evident phase segregation through appearance of those small holes. Boiling temperature for TOTM is 414 °C, much higher than that employed for extrusion and even higher than that displayed by ATBC. Consequently, these cavities cannot be attributed to the evaporation occurred during processing but to its incomplete solubility into the PLA matrix. On the other hand, a homogeneous distribution of MCM-41 particles is observed in both ternary materials, independently of the plasticizer used. Furthermore, inorganic domains of considerable size are not exhibited and, consequently, a significant role as nucleating agent can be expected.

Figure 3 shows the DSC first heating curves at 10 °C/min of the different compressed-molded materials. Several phase transitions can be observed in order of increasing temperatures: glass transition, cold crystallization and melting processes. In all the cases, the neat enthalpy from the whole DSC curve for all of the samples is practically zero, meaning that these initial materials, prepared by compression molding

and rapidly cooled from the melt, are completely amorphous. Regarding the glass transition,  $T_g$ , its temperature location shows a very important depression when the ATBC plasticizer is added, as seen in the PLAM0A10 specimen. This  $T_g$  displacement is rather analogous to the one previously reported in bibliography [9, 33], associated with a good solubility of ATBC within PLA, which may be different to the one for TOTM. Furthermore, since the  $T_g$  of PLAM5A10 is lower than that of PLAM0A10, then an additional decrease in  $T_g$  is exhibited if MCM-41 is included as nucleant.

A reduction in  $T_g$  is also noticeable in the case of incorporating the TOTM as plasticizer in the binary PLAM0T10 blend, although displacement of the  $T_g$  temperature is significantly smaller than that noted when the ATBC is used as additive. Moreover, the MCM-41 addition does not lead now to a supplementary reduction of  $T_g$  in the PLAM5T10 composite. For the PLAM5 sample, the value of  $T_g$  is, however, practically the same than that for neat PLA.

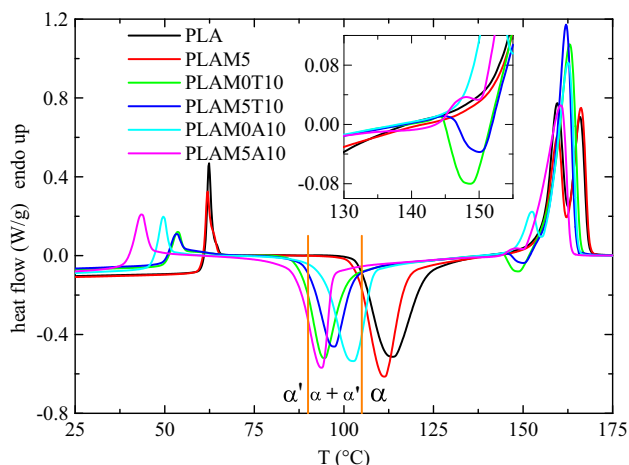


**Figure 3** DSC first melting curves at 10 °C/min of the different compressed-molded materials. The curves for samples PLA, PLAM5, PLAM0A10 and PLAM5A10 have been taken from reference [19]. The vertical lines are the corresponding values reported in reference [27], exhibiting the temperature ranges where the pure  $\alpha'$  or  $\alpha$  modifications are expected to be developed (or the interval where both forms coexist) in this PLA under analysis. The inset shows an amplification in the region of the  $\alpha'$  to  $\alpha$  transition.

All these  $T_g$  changes have been quantified and are represented in Fig. 4c.

Similarly to the  $T_g$  characteristics, the cold PLA crystallization process ( $T_{cc}^{F1}$ ) is strongly dependent on the presence of plasticizer (ATBC or TOTM), of MCM-41 or of the joint action of both, plasticizer and mesoporous silica. All of the materials containing plasticizer, either ATBC or TOTM, crystallize more rapidly than the neat PLA. The same feature is observed when MCM-41 is incorporated, either in the binary or the ternary composites. This aspect, evident in the dynamic measurements represented in Fig. 3, will be also confirmed below when analyzing the isothermal crystallization rates. Nevertheless, an opposite trend is noticed in the binary blends and the ternary composites as function of the type of plasticizer added, as deduced from Fig. 3. Thus, the PLAM0T10 specimen shows a  $T_{cc}^{F1}$  displacement greater than that noted for the PLAM0A10 blend (see Figs. 3, 4b), which can be attributed to the more rigid chemical structure of the TOTM plasticizer that can nucleate more favorably the PLA crystallization. The  $T_{cc}^{F1}$  is, however, found in PLAM5A10 at temperature lower than in PLAM5T10, indicating the more positive interactions between ATBC/MCM-41

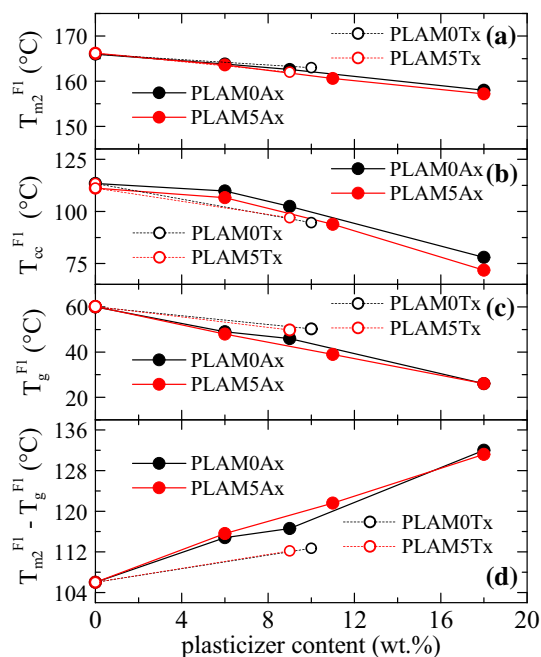


**Figure 4** Variation with the plasticizer content, in the first heating run, of: **a** the second melting temperature; **b** the cold crystallization; **c** the glass transition temperature, and **d** the difference between the second melting temperature and the glass transition, for the different specimens. Data for samples PLA, PLAM5, PLAM0Ax and PLAM5Ax have been taken from reference [19].

with PLA in the PLAM5A10 than between TOTM/MCM-41 with PLA in the PLAM5T10 ternary system.

Concerning the melting process, PLA and PLAM5 samples show a clear bimodal contour of this endotherm, characterized by the  $T_{m1}^{F1}$  and  $T_{m2}^{F1}$  melting temperatures at low and high temperature, respectively, while those ones incorporating TOTM, PLAM0T10 and PLAM5T10, display a unique peak after an exothermic event that occurs just before the main melting starts. The PLAM0A10 and PLAM5A10 specimens also show only one main peak although a small endotherm is observed below its beginning, being of higher intensity in PLAM0A10 than in PLAM5A10. These double melting peaks noticed in some of the samples are attributed to two populations of crystallites: on one hand, the melting of crystals ( $T_{m1}^{F1}$ ) developed during cold crystallization on heating; and, on the other hand, the  $T_{m2}^{F1}$  event, which is ascribed to the melting of the thickening entities, is able to recrystallize after their initial melting (see Fig. 4a). Thus, a melt-recrystallization of PLA is the prevailing process that

takes place in these systems [34–36] because their  $T_{cc}^{F1}$  is above 105 °C, *i.e.*, above the orange vertical line located at the highest temperature in Fig. 3.

These vertical lines correspond to the temperature intervals, reported in reference [27], where the pure  $\alpha'$  or  $\alpha$  modifications are expected to be formed (or the range where both forms coexist) for this PLA under analysis, composed by a content of around 2 mol % in *D* stereoisomer. Then, it is observed that specimens PLA and PLAM5 show the  $T_{cc}^{F1}$  in the region where only the  $\alpha$  modification is anticipated. For the other samples with plasticizer, the  $T_{cc}^{F1}$  is located in the interval where the two forms,  $\alpha'$  and  $\alpha$ , are expected to be developed, although location of  $T_{cc}^{F1}$  in the PLAM0A10 specimen is rather close to the region of formation for the pure  $\alpha$  form. It is well known that when  $\alpha'$  crystals are present, they show a transformation from the  $\alpha'$  to the  $\alpha$  modification during the heating process, characterized by a small exotherm just before the primary melting process [29, 30, 37, 38]. The results in Fig. 3 show very undoubtedly this  $\alpha' \rightarrow \alpha$  crystal transformation for samples PLAM0T10 and PLAM5T10, at around 140–150 °C (and only very slightly for PLAM5A10, as observed in the inset of Fig. 3). In fact, those two specimens display only the second melting temperature, as aforementioned, while the two processes of  $T_{m1}^{F1}$  and  $T_{m2}^{F1}$  are noted for the other samples in Fig. 3. It seems, therefore, that the presence of TOTM is particularly sensitive to the observation of the  $\alpha'$  to  $\alpha$  transition. We plan to study this aspect in more detail by performing diffraction experiments with synchrotron radiation, analyzing the regions at small and wide angles, especially when the  $\alpha'$  modification is obtained (see below).

Regarding the  $T_{m2}^{F1}$ , a decrease is, however, shown when comparing that for the neat PLA and the values exhibited by the materials with plasticizers (see Figs. 3, 4a). Anyway, the displacement for the melting temperatures is much smaller than the one noticed for  $T_g$  values, so that the difference between the melting temperatures and the glass transition ones increases considerably by adding the two plasticizers, as observed in Fig. 4d, being smaller, but rather significant, in the case of using the TOTM plasticizer. It means that the interval for crystallization temperatures is expected to be enlarged rather appreciably when the plasticizers are present since that difference is directly related to the actual crystallization window.

The higher crystallization rate anticipated from the results in Fig. 3 for the plasticized samples, either binary or ternary systems, is also deduced from Fig. 5a, which shows the cooling curves from the melt, at 10 °C/min. The pristine PLA specimen does not show any crystallization at that relatively low cooling rate. On the contrary, all the other samples exhibit an evident crystallization exotherm, with more or less intensity.

The corresponding values of the DSC crystallinity deduced from those exotherms (and normalized to the actual PLA content in the samples) are plotted in Fig. 5b, where it can be noted that the degree of crystallinity for the two samples with the TOTM plasticizer is significantly higher than the one for PLA or PLAM5, although considerably higher values are obtained in the specimens with ATBC. This feature can be ascribed to the morphological differences, depicted in Fig. 2, existing in the materials that incorporate ATBC or TOTM. A suitable solubility of the former within the PLA leads to a more efficient effect on the formation of crystals, promoting a larger degree of crystallinity. The TOTM influence is, however, inferior because its solubility is not so complete.

A thoroughly detailed study of the role of addition of MCM-41 and ATBC or TOTM on the PLA crystallization rate has been performed by isothermal crystallization experiments, both from the glassy or from the melt states. Obviously, the crystallization from the glass is much faster than the one from the melt [4].

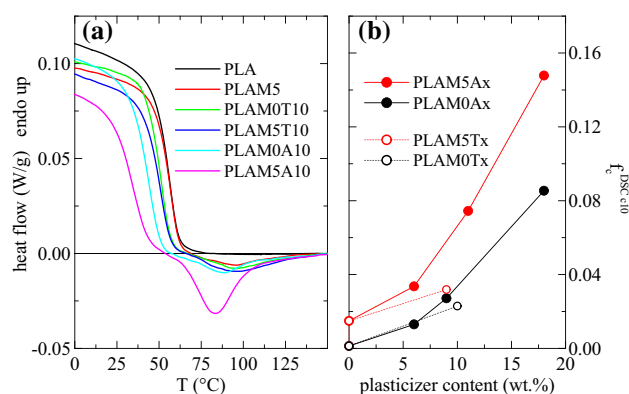


**Figure 5** **a** DSC cooling curves from the melt, at 10 °C/min, for the different samples; and **b** corresponding DSC crystallinity, normalized to the actual PLA content in the sample, as a function of the plasticizer content. Data for samples PLA, PLAM5, PLAM0A10 and PLAM5A10 have been taken from reference [19].



In fact, observation of the isotherms from the glass above around 100 °C was not possible in a previous paper [19] because the crystallization rate was so fast that it occurred during the preliminary heating for reaching the crystallization temperature. Those experiments were carried out at 60 °C/min, while the heating rate has been increased up to 120 °C/min in these present measurements. Using this higher rate, the crystallization from the glass has been performed, and observed, in the entire crystallization window, with only one exception. Thus, Fig. 6 shows the DSC heating curves from the glassy state for samples PLAM5T10 and PLAM5A10, at 60 °C/min (Fig. 6a) and at 120 °C/min (Fig. 6b). It can be deduced that the isotherms are expected to be correct at 60 °C/min up to a crystallization temperature of around 115 °C for PLAM5T10, and only up to about 100 °C for specimen PLAM5A10. On the contrary, by using 120 °C/min, specimen PLAM5T10 keeps practically amorphous for the whole experiment, and, therefore, the isothermal crystallization can be evaluated at any temperature in the crystallization window. Sample PLAM5A10, however, presents a clear (although of small intensity) cold crystallization above around 120 °C, so that the isotherms shall not be accurate above that temperature. The normalized enthalpies involved in the cold crystallization of this sample are 42.3, 25.6 and 5.1 J/g

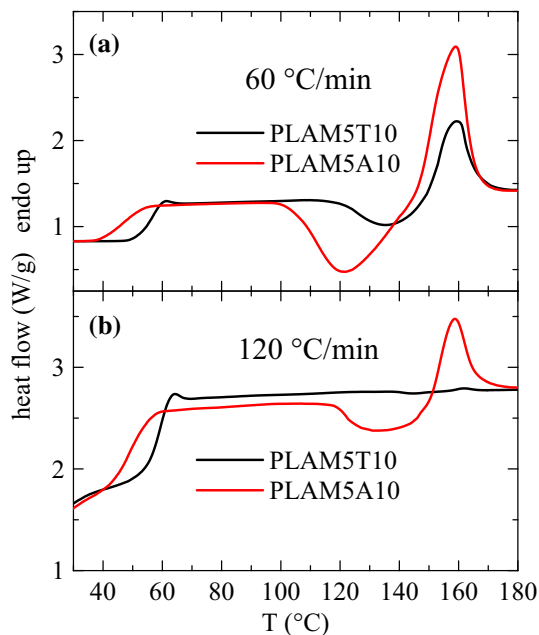


**Figure 6** DSC heating curves from the glassy state for samples PLAM5T10 and PLAM5A10, at 60 °C/min (a) and 120 °C/min (b)

when using heating rates of 10, 60 and 120 °C/min, respectively, as deduced from Figs. 3, 6a, b.

Crystallization rate can be quantified for these isothermal crystallizations, either from the melt or from the glass, from the inverse of the time needed for obtaining a 50% transformation in the isotherms, *i.e.*, the half-crystallization time,  $t_{0.5}$ . These values of  $1/t_{0.5}$  for the different materials and for the two modes of crystallization are represented in Fig. 7. The results from the glass are shown in Fig. 7a, while those from the melt, in Fig. 7b, where the Y scale has been amplified 5 times in relation to Fig. 7a, owing to the much lower crystallization rates when crystallizing from the melt. As mentioned above, the heating rate used for reaching the isothermal temperature in the crystallizations from the glass has been 120 °C/min, and then, the results show also the typical maxima in the crystallization rate (Fig. 7a), arising from the well-known two factors, the transport term and the free-energy one, which govern the crystallization rate of polymers [39, 40], both terms showing opposite temperature coefficients. The maximum is not noticeable, however, for sample PLAM5A10, since, as shown above in Fig. 6b, a cold crystallization is noted even when using a heating rate of 120 °C/min, beginning at around 120 °C, so that the isotherms cannot be properly observed above that crystallization temperature.

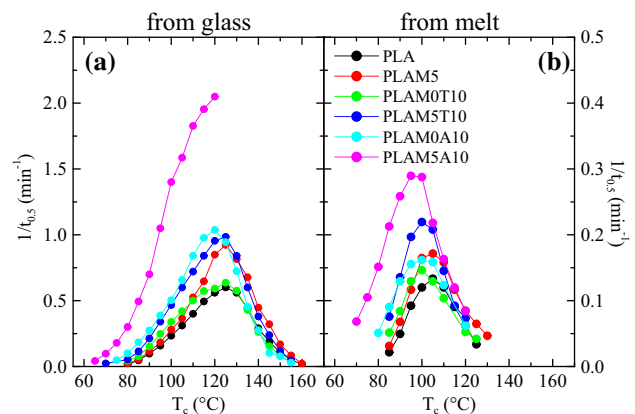


**Figure 7** Variation with  $T_c$  of the inverse of the half-crystallization time in the isotherms for the different samples, when isothermally crystallized from the glass (a) and from the melt (b). The Y scale in the results from melt has been amplified 5 times. Data for samples PLA, PLAM5, PLAM0A10 and PLAM5A10 crystallized from the melt have been taken from reference [19].

It might be logical to expect that the maximum could be detected just by increasing the heating rate even more. Nevertheless, higher values are not possible because then the time needed for isothermal temperature equilibration becomes on the order (or greater) than the required one for the isothermal crystallization. It can be also deduced from Fig. 7 that the possible presence of two different maxima, one related to development of the  $\alpha'$  form and another for formation of the more ordered  $\alpha$  modification, cannot be clearly detected, neither in the results from the glass, nor in those from the melt.

Figure 8 represents the variation of the maximum rate coordinates, in the isotherms from the melt, with the plasticizer content for the two series of materials with different plasticizer. It can be observed that the two samples containing the TOTM plasticizer show significantly higher values of  $1/t_{0.5}^{\max}$  in relation to those for the PLA or PLAM5 specimens, as happened with the crystallinity in Fig. 5b, but they are considerably lower than those shown by the specimens with ATBC, at a given plasticizer content. The values for

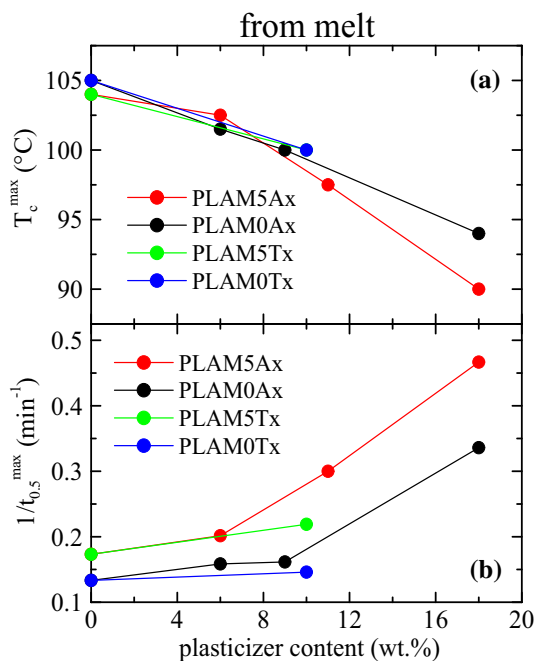


**Figure 8** Dependence on the plasticizer content in the materials of the maximum rate coordinates in the isotherms from the melt for the two series of samples: **a** crystallization temperature at the maximum and **b** inverse half-crystallization time. Data for samples PLA, PLAM5, PLAM0Ax and PLAM5Ax have been taken from reference [19].

$T_c^{\max}$  are, however, somewhat more similar, especially for the case of PLAM0Tx and PLAM0Ax (Fig. 8a).

It was suggested in a previous study [19] that there was a synergistic effect between the MCM-41 mesoporous silica and the ATBC plasticizer on the nucleation ability of PLA, resulting on significantly greater crystallization rates (and also extending significantly the crystallization window). This is actually deduced from Fig. 8b by observing the increasingly higher difference in the maximum rate between the series PLAM5Ax and PLAM0Ax. Despite the reduced number of samples in the set with TOTM, this feature seems to be also noticeable, since the difference in  $1/t_{0.5}^{\max}$  between PLAM5T10 and PLAM5 is higher than that between PLAM0T10 and PLA.

Figure 9 presents the DSC heating curves after isothermal crystallization from the melt at two temperatures: 85 (i85) and 90 °C (i90). These two crystallization temperatures have been selected because the  $\alpha'$  to  $\alpha$  transition is observed in the different samples analyzed. In fact, the corresponding amplifications in the region of that crystal  $\rightarrow$  crystal transition are shown in the right plots of Fig. 9. These curves show the important differences found between composites incorporating the two different plasticizers. Thus, the TOTM samples show very evidently, similar to samples PLA and PLAM5, the transition from the  $\alpha'$  lattice to the  $\alpha$  form, through the manifestation of the exotherm event just before the primary melting process [29, 30, 37, 38], while this transition appears wider and of smaller intensity in the specimens with ATBC. These results seem to point out that development of the  $\alpha'$  polymorph is hindered in the materials where ATBC plasticizer is added, more in the ternary composites than in the binary blends. The combined presence of MCM-41 and ATBC appears to boost the formation of the more ordered  $\alpha$  phase.

Figure 10 represents the variation with  $T_c$  of the temperature for the transition from the  $\alpha'$  to the  $\alpha$  polymorph for the different samples, after isothermal crystallization from either the glassy or the molten states. The results for samples PLA, PLAM5, PLAM0A10 and PLAM5A10 crystallized from the melt have been taken from reference [19]. Those data for the crystallization from the glass are all new results since the experiments for this comparative research have been performed using a heating rate of 120 °C/min to reach the isothermal crystallization temperature. First of all, it can be observed that the results from the glass and from the melt are rather similar for

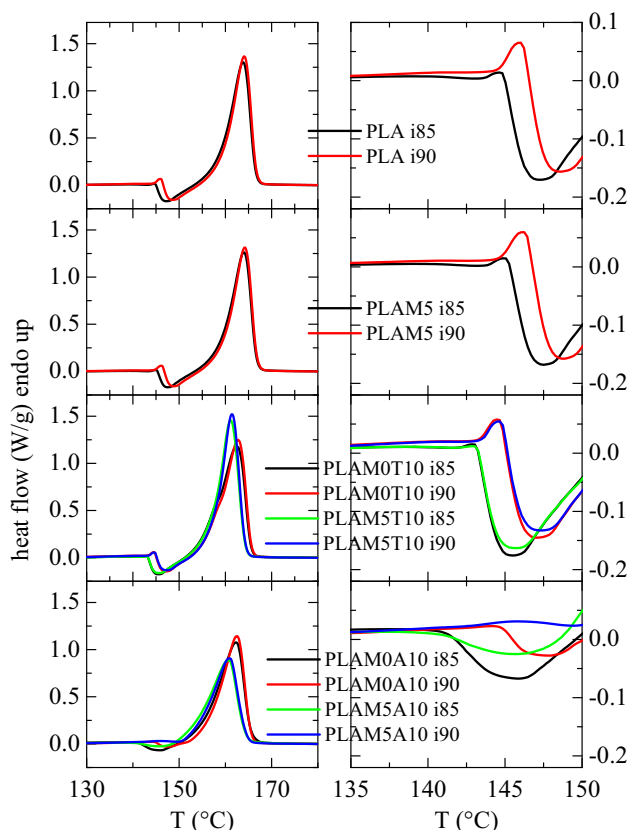


**Figure 9** Left frames: DSC heating curves, at 10 °C/min, for the indicated samples after isothermal crystallization from the melt at 85 (i85) and 90 °C (i90). Right frames: corresponding amplifications in the region of the transition from  $\alpha'$  to  $\alpha$ . Data for samples PLA, PLAM5, PLAM0A10 and PLAM5A10 have been taken from reference [19].

the different samples. Obviously, data from the glass extend to lower crystallization temperatures, because the considerably smaller rates attained when crystallizing from the melt preclude the observation of the corresponding isotherms at those lower temperatures due to the rapid deterioration of signal-to-noise ratio in the isotherms with increasing crystallization times.

A second aspect deduced from Fig. 10 is that the samples containing plasticizer show considerably lower values for the temperature of  $\alpha' \rightarrow \alpha$  transition while PLA and PLAM5 specimens behave rather similar. The results for the specimens with TOTM appear to be intermediate between the ones for PLA (or PLAM5) and those shown by specimens that incorporate the ATBC plasticizer. This intermediate behavior stands also for the extension of available crystallization temperatures to lower values. Obviously, these available temperatures simply

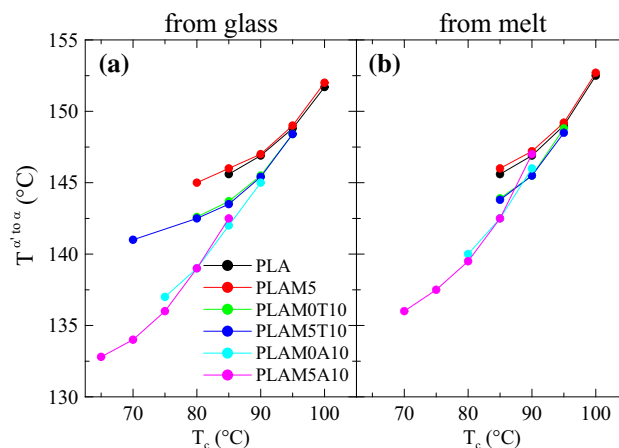


**Figure 10** Variation with  $T_c$  of the temperature for the transition from  $\alpha'$  to  $\alpha$  polymorph for the different samples, after isothermal crystallization from the glass (a), and from the melt (b). Data for samples PLA, PLAM5, PLAM0A10 and PLAM5A10 crystallized from the melt have been taken from reference [19].

reflect the corresponding increase in crystallization rates, so that the isotherms can be observed at lower values of crystallization temperatures with sufficient signal-to-noise ratio.

As an example of the curves for all the crystallization temperatures, Fig. 11 shows the DSC heating curves, at 10 °C/min, for sample PLAM5T10 after isothermal crystallization from the glassy state. Three regions can be discerned. The first one, up to around  $T_c$  of 100 °C, is characterized by presence of the disordered  $\alpha'$  modification, which has been developed at the lowest crystallization temperatures. Thus, the  $\alpha'$  to  $\alpha$  transition is noticeable on melting, followed by the melting of those recrystallized and more ordered  $\alpha$  crystallites, which takes place finally at around 160–165 °C. This later endotherm will be termed as  $T_{m2}$ , since it represents the melting of the recrystallized crystals, and not that for the ones originally formed.

The second region, noted at values of  $T_c$  from around 105 to 125 °C, represents the cases where, mostly or totally, the  $\alpha$  modification is initially present, and two melting endotherms can be observed. The first one,  $T_{m1}$ , is ascribed to the melting of the original not very perfect  $\alpha$  crystals developed during the isothermal crystallization, so that they can

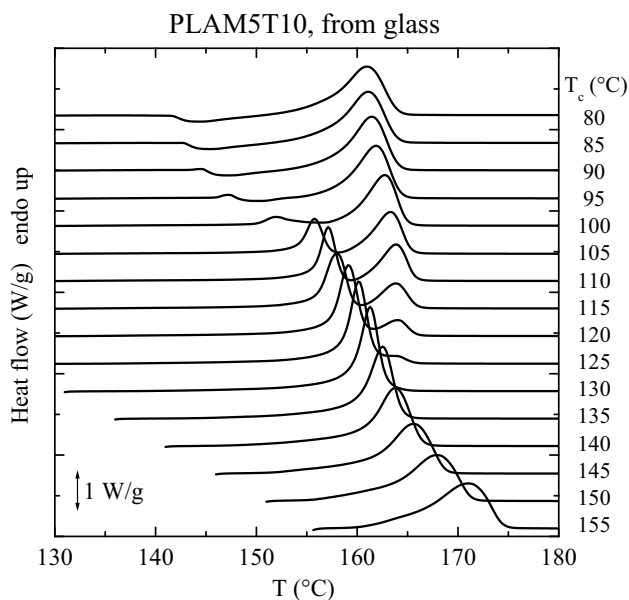


**Figure 11** DSC heating curves, at 10 °C/min, for sample PLAM5T10 after isothermal crystallization from the glassy state at the indicated temperatures.

recrystallize on melting into more perfect crystallites, giving rise to the second melting endotherm,  $T_{m2}$ .

Finally, the third scenario is noticed at the highest values of  $T_c$ . Appearance of a single melting endotherm is now observed since the  $\alpha$  crystals generated at those high isothermal temperatures are already rather perfect and do not undergo any further recrystallization. The temperature at maximum represents the true melting temperature,  $T_{m1}$ .

Figure 12 depicts the values of the two melting temperatures exhibited by all the samples here analyzed, after isothermal crystallization from the glass, as a function of  $T_c$ . It can be observed that the values of  $T_{m1}$  at low crystallization temperatures show an abnormally great decrease, what is attributed to the fact that formation of both  $\alpha'$  and  $\alpha$  crystals took place at those temperatures, *i.e.*, there is coexistence of these two polymorphs. Consequently, two different processes overlapped in that  $T_{m1}$  and its differentiation is not easy. On one hand, the  $\alpha'$  crystals undergo its melting and further recrystallization into the  $\alpha$  modification, and, on the other hand, the initial  $\alpha$  crystallites show its own value of  $T_{m1}$ .

At intermediate  $T_c$  corresponding to the second region in Fig. 11, the values of  $T_{m1}$  show a continuous increase, giving rise also to the observation of  $T_{m2}$ , which shows approximately constant values in

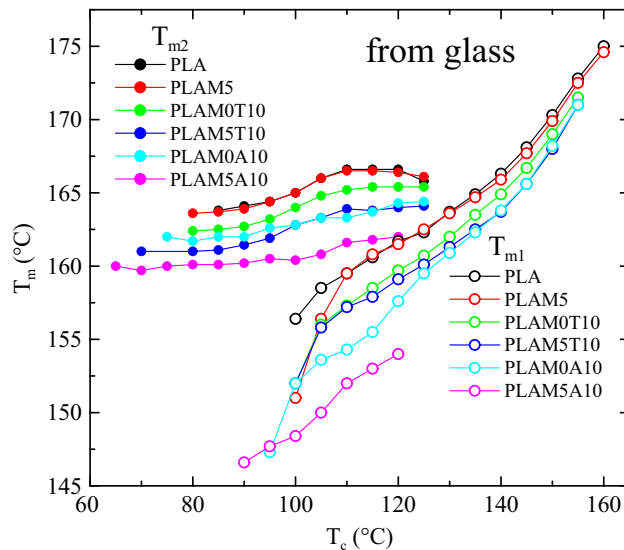


**Figure 12** Dependence on  $T_c$  of the melting temperatures for the different samples, after isothermal crystallization from the glass.

that interval. And for the highest values of  $T_c$  the endotherm  $T_{m2}$  disappears and only  $T_{m1}$  is observed, showing an even higher dependence with  $T_c$ , with values of the slope close to 0.5, as it usually happens in the crystallization of polymer systems [40, 41].

Regarding the variation of  $T_{m2}$  on  $T_c$  there are two appreciable trends. The one at the lower values of  $T_c$ , where the  $\alpha'$  modification is present, shows values of  $T_{m2}$  around 2–3 °C below those corresponding to the  $\alpha$  form, which is developed at higher crystallization temperatures.

Another important aspect from Fig. 12 is the comparison of the melting temperatures for the different samples. It can be observed that specimens PLA and PLAM5 show very similar values of the different transition temperatures, while the  $T_{m,s}$ , either  $T_{m1}$  or  $T_{m2}$ , for all the other samples display lower values (it should be said that this decrease is not as high as that exhibited by the  $T_{g'}$ , as deduced from Fig. 2). Thus, the order of melting temperatures is the following: PLA = PLAM5 > PLAM0T10 > PLAM0A10 = PLAM5T10 > PLAM5A10. In fact, PLAM0A10 and PLAM5T10 really display similar values of  $T_{m1}$  and  $T_{m2}$  at high values of  $T_c$  but at lower crystallization temperatures, the behavior is not so clear, with  $T_{m1}$  being higher for PLAM5T10, and  $T_{m2}$  for PLAM0A10.

Despite that reduction in the melting temperatures, the crystallinity developed by the different

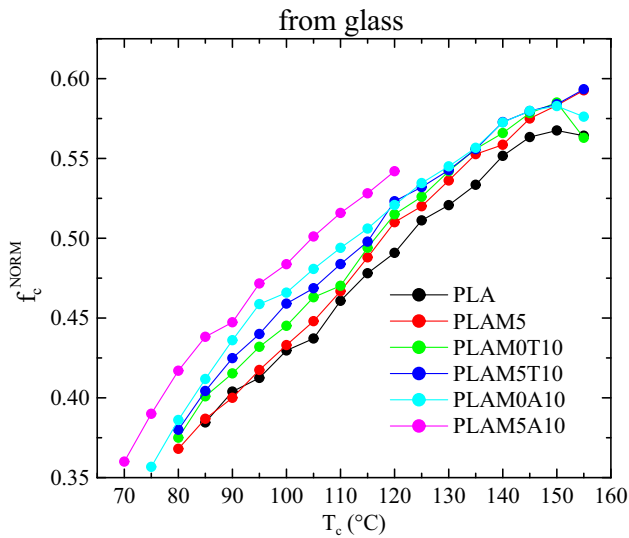


**Figure 13** Dependence on  $T_c$  of the DSC crystallinity (normalized to the actual PLA content) for the different samples, after isothermal crystallization from the glass.

materials displays an opposite order, as noticed in Fig. 13, which represents the variation with  $T_c$  of the DSC crystallinity (normalized to the actual PLA content) for the different samples, after isothermal crystallization from the glass. Thus, the degree of crystallinity is always higher for the specimens with plasticizer, as it happened also with the crystallization rates.

These results indicate, therefore, that incorporation of these two plasticizers, TOTM or ATBC, leads to an increase in the crystallization rate of PLA and in its degree of crystallinity, despite values of the melting temperatures are smaller. Moreover, somewhat intermediate values between neat PLA and the ones for the ATBC samples are observed for the TOTM specimens, either the binary blend or the ternary composite, for the crystallization rate, the transition temperatures or the amount of crystallites developed during crystallization.

At this point, it is important to indicate that those segments of the macrochains located in the amorphous regions close to the crystallites are more constrained than those that are further away, the former giving rise to the so-called rigid amorphous fraction (RAF) and the latest to the mobile amorphous fraction (MAF) [42, 43]. It has been shown [43] that, when crystallizing, the ATBC concentration in the MAF increases somewhat,

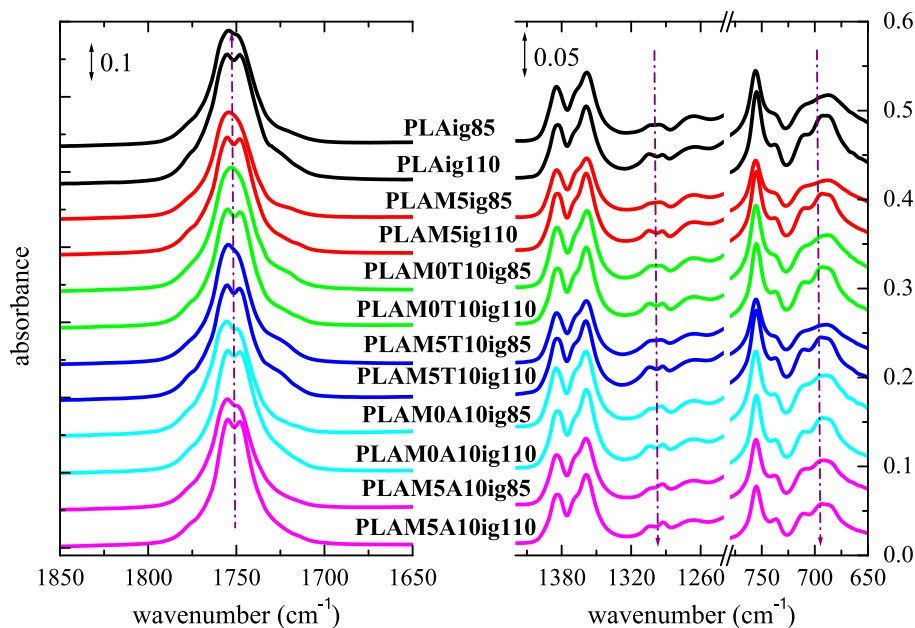
so that its content diminishes accordingly in the RAF. One of the possible reasons for the dissimilar behavior between TOTM and ATBC composites could be a different partitioning of the two plasticizers in those amorphous fractions, which may be dependent upon specific chemical interactions and/or steric hindrances. As a result, the mobility of PLA chains may be somewhat different among the two systems.

Assumptions made from the DSC results concerning the type of crystal lattice developed during isothermal crystallizations are confirmed by FTIR measurements performed on each material annealed from the amorphous glassy state at two different temperatures, 85 and 110 °C, since infrared spectroscopy turned out a noteworthy tool for PLA structural characterization [30, 44]. Additionally, we plan to perform X-ray experiments with synchrotron radiation in the future on these samples in order to, eventually, analyze possible differences in the degree of order of these two crystalline phases ( $\alpha'$  and  $\alpha$ ) among the different materials, paying special attention to the case of the  $\alpha'$  modification.

Figure 14 displays the FTIR spectra attained. Several regions have been selected [45, 46]: on one hand, the C=O stretching band due to its conformational sensitivity (represented on the left) and, on the other hand, two spectral zones on the right plot related to scissoring motions of the methyl groups and specific bending modes from the C=O, located in the interval of wavenumber ranging from 1420 to 1240  $\text{cm}^{-1}$  and from 800 to 650  $\text{cm}^{-1}$ , respectively.

Samples of the distinct materials isothermally crystallized from the amorphous glass at the lowest temperature, *i.e.*, at 85 °C, are characterized by observation of broad peaks in these wavenumber intervals analyzed, while the splitting of some of those IR modes is evident in those annealed at 110 °C. This split is ascribed to specific carbonyl and methyl interactions existing in the  $\alpha$  polymorph that are not present in the  $\alpha'$  phase [44]. The crystalline polymorphs developed during crystallization at these two temperatures are not the same, since the  $\alpha'$  lattice is majorly attained at 85 °C, with the exception of PLAM0A10ig85 and PLAM5A10ig85 where the  $\alpha$  phase seems to be also in majority, while the  $\alpha$  form is generated at 110 °C [27]. These differences in the chain interactions and their packing promote a greater ordering in the  $\alpha$  lattice, which leads to the greater resolution of the IR bands

**Figure 14** Carbonyl stretching band (left) and bending region for scissoring motions of the methyl groups as well as for C=O (right) in the different materials isothermally crystallized from the glassy state at 85 (ig85) and 110 °C (ig110).



noticed in the materials crystallized at 110 °C, as seen in Fig. 14.

## Conclusions

Binary blends based on an *L*-rich PLA and two different plasticizers, TOTM or ATBC, have been prepared by melt extrusion together with their corresponding composites with a 5 wt.% of mesoporous MCM-41 silica, which acts as crystallization nucleant. Mesoporous particles are observed to be suitably distributed within the bulk of composites, although fracture surface is very dissimilar depending upon the plasticizer incorporated. Numerous voids are noted in the PLAM5T10 composite containing TOTM while a rather continuous surface is exhibited by in the PLAM5A10 ternary system.

Main features found in the several phase transitions during the first heating process under dynamic conditions for the different materials are the following: (a) glass transition is remarkably shifted to lower temperatures as the ATBC is added (mainly in the PLAM5A10 composite) while this displacement is smaller in the materials (either binary or ternary) containing TOTM; (b) cold crystallization of PLA is also considerably affected by addition of TOTM or ATBC, moving its location down to inferior temperatures compared with that exhibited by the neat

matrix. Accordingly, presence of plasticizer enables a faster PLA crystallization, ATBC being more efficient than TOTM in the ternary composites; and, (c)  $\alpha' \rightarrow \alpha$  transformation is more evident in the materials that incorporate TOTM, indicating that presence of ATBC favors the formation of the  $\alpha$  form. FTIR spectroscopy experiments have been also performed in order to confirm the development of each one of the two PLA polymorphs: disordered  $\alpha'$  or ordered  $\alpha$  form.

The maximum rate in the PLA crystallization is observed at about 95–105 °C in the measurements from the melt, showing this rate a remarkable increase with the combined effect of plasticizer and MCM-41 particles. The influence is more relevant in the system with ATBC. In the samples crystallized from the glass, that maximum in the rate appears at higher temperatures, ranging from 115 to 125 °C. Its observation has been possible by using a rate as high as 120 °C/min for the heating from the glassy state to the crystallization temperature.

Presence of TOTM or ATBC and the mesoporous MCM-41 particles also implies an increase in the crystallinity of PLA. As in the rate of crystallization, ATBC is more effective than TOTM.

One of the possible reasons for the dissimilar behavior observed in the composites incorporating TOTM and those based on ATBC could be a different partitioning of these two plasticizers in the two types of amorphous fractions, RAF and MAF.

Summarizing, the combined action of plasticizer (TOTM or ATBC) and MCM-41 particles enables a considerable improvement in the mobility of PLA chains, affecting glass transition as well as crystallization rate and leading to a widening of the PLA window for its three-dimensional ordering. Therefore, ultimate requirements can be easily tuned contributing to spread out the PLA applications.

## Acknowledgements

This research was funded by MCIN/AEI/<https://doi.org/10.13039/501100011033>, grant number PID2020-114930GB-I00. Grant BES-2017-082284 was also funded by MCIN/AEI/ <https://doi.org/10.13039/501100011033> and, thus, TMDR is also thankful for this pre-doctoral funding. Authors are, additionally, grateful to the Characterization Service for SEM and TGA facilities and to the Service of Physicochemical Characterization of Polymers for DSC experiments, both services belonging to ICTP-CSIC as well as to the personnel of these two Services for the support.

## Author contributions

EBB contributed to conceptualization, methodology, investigation, formal analysis, and writing—review and editing; RBG contributed to methodology, investigation, and writing—review and editing; TMDR contributed to investigation and writing—review and editing; MLC contributed to conceptualization, methodology, investigation, resources, writing—original draft preparation, writing—review and editing, project administration, supervision, and funding acquisition; EP contributed to conceptualization, methodology, software, formal analysis, investigation, resources, writing—original draft preparation, writing—review and editing, and funding acquisition. All authors have read and agreed to the published version of the manuscript.

## Funding

Open Access funding provided thanks to the CRUE-CSIC agreement with Springer Nature.

## Data availability

Data are contained within the article.

## Declarations

**Conflict of interest** The authors declare no conflict of interest.

**Open Access** This article is licensed under a Creative Commons Attribution 4.0 International License, which permits use, sharing, adaptation, distribution and reproduction in any medium or format, as long as you give appropriate credit to the original author(s) and the source, provide a link to the Creative Commons licence, and indicate if changes were made. The images or other third party material in this article are included in the article's Creative Commons licence, unless indicated otherwise in a credit line to the material. If material is not included in the article's Creative Commons licence and your intended use is not permitted by statutory regulation or exceeds the permitted use, you will need to obtain permission directly from the copyright holder. To view a copy of this licence, visit <http://creativecommons.org/licenses/by/4.0/>.

## References

- [1] Celebi H, Gunes E (2018) Combined effect of a plasticizer and carvacrol and thymol on the mechanical, thermal, morphological properties of poly(lactic acid). *J Appl Polym Sci* 135:45895
- [2] Saeidlou S, Huneault MA, Li H, Park CB (2012) Poly(lactic acid) crystallization. *Prog Polym Sci* 37:1657–1677
- [3] Petchwattana N, Narupai B (2019) Synergistic effect of talc and titanium dioxide on poly(lactic acid) crystallization: an investigation on the injection molding cycle time reduction. *J Polym Environm* 27:837–846
- [4] Díez-Rodríguez TM, Blázquez-Blázquez E, Pérez E, Cerrada ML (2020) Composites based on poly(lactic acid) (PLA) and SBA-15: effect of mesoporous silica on thermal stability and on isothermal crystallization from either glass or molten state. *Polymers* 12:2743
- [5] Díez-Rodríguez TM, Blázquez-Blázquez E, Martínez JC, Pérez E, Cerrada ML (2022) Composites of a PLA with

- SBA-15 mesoporous silica: Polymorphism and properties after isothermal cold crystallization. *Polymer* 241:124515
- [6] Díez-Rodríguez TM, Blázquez-Blázquez E, Barranco-García R, Pérez E, Cerrada ML (2022) Synergistic effect of mesoporous SBA-15 particles and processing strategy for improving PLA crystallization capability in their composites. *Macromol Mater Eng* 307:2200308
- [7] Zhao DY, Feng JL, Huo QS, Melosh N, Fredrickson GH, Chmelka BF, Stucky GD (1998) Triblock copolymer syntheses of mesoporous silica with periodic 50 to 300 angstrom pores. *Science* 279:548–552
- [8] Loudin D, Bizot H, Colonna P (1997) “Anti-plasticization” in starch-glycerol films? *J Appl Polym Sci* 63:1047–1053
- [9] Maiza M, Benaniba MT, Massardier-Nageotte V (2016) Plasticizing effects of citrate esters on properties of poly(lactic acid). *J Polym Eng* 36:371–380
- [10] Ljungberg N, Wesslén B (2005) Preparation and properties of plasticized poly(lactide) films. *Biomacromol* 6:1789–1796
- [11] Jacobsen S, Fritz HG (1999) Plasticizing poly(lactide)-the effect of different plasticizers on the mechanical properties. *Polym Eng Sci* 39:1303–1310
- [12] Focarete ML, Dobrzynski MS, Kowalczyk M (2002) Miscibility and mechanical properties of blends of (l)-lactide copolymers with atactic poly(3-hydroxybutyrate). *Macromolecules* 35:8472–8477
- [13] Blümm E, Owen AJ (1995) Miscibility, crystallization and melting of poly(3-hydroxybutyrate)/poly(L-lactide) blends. *Polymer* 36:4077–4081
- [14] Hu Y, Hu YS, Topolkaev V, Hiltner A, Baer E (2003) Crystallization and phase separation in blends of high stereoregular poly(lactide) with poly(ethylene glycol). *Polymer* 44:5681–5689
- [15] Hu Y, Rogunova M, Topolkaev V, Hiltner A, Baer E (2003) Ageing of poly(lactide)/poly(ethylene glycol) blends. part 1. poly(lactide) with low stereoregularity. *Polymer* 44:5701–5710
- [16] Kulinski Z, Piorkowska E, Gadzinowska K, Stasiak M (2006) Plasticization of poly(lactide) with poly(propylene glycol). *Biomacromol* 7:2128–2135
- [17] Ljungberg N, Andersson T, Wesslén B (2003) Film extrusion and film weldability of poly(lactide) plasticized with triacetin and tributyl citrate. *J Appl Polym Sci* 88:3239–3247
- [18] Ljungberg N, Wesslén B (2003) Tributyl citrate oligomers as plasticizers for poly(lactide): thermo-mechanical film properties and aging. *Polymer* 44:7679–7688
- [19] Blázquez-Blázquez E, Barranco-García R, Díez-Rodríguez TM, Cerrada ML, Pérez E (2023) Combined effects from dual incorporation of ATBC as plasticizer and mesoporous MCM-41 as nucleating agent on the PLA isothermal crystallization in environmentally-friendly ternary composite systems. *Polymers* 15:624
- [20] Beck JS, Vartuli JC, Roth WJ, Leonowicz ME, Kresge CT, Schmitt KD, Chu CT-W, Olson DH, Sheppard EW, McCullen SB, Higgins JB, Schlenker JL (1992) A new family of mesoporous molecular sieves prepared with liquid crystal templates. *J Am Chem Soc* 114:10834
- [21] Ren Z, Dong L, Yang Y (2006) Dynamic mechanical and thermal properties of plasticized poly(lactic acid). *J Appl Polym Sci* 101:1583–1590
- [22] Blázquez-Blázquez E, Barranco-García R, Cerrada ML, Pérez E (2019) Effect of thermo-oxidation on loss of plasticizers, on crystalline features and on properties in a metalocene isotactic polypropylene. *Polymer* 181:121749
- [23] Li HB, Huneault MA (2007) Effect of nucleation and plasticization on the crystallization of poly(lactic acid). *Polymer* 48:6855–6866
- [24] Li Y, Wu H, Wang Y, Liu Li, Han L, Wu J, Xiang F (2010) Synergistic effects of PEG and MWCNTs on crystallization behavior of PLLA. *J Polym Sci Part B: Polym Phys* 48:520–528
- [25] Scatto M, Salmini E, Castiello S, Coltelli MB, Conzatti L, Stagnaro P, Andreotti L, Bronco S (2013) Plasticized and nanofilled poly(lactic acid)-based cast films: effect of plasticizer and organoclay on processability and final properties. *J Appl Polym Sci* 127:4947–4956
- [26] Shi X, Zhang G, Phuong TV, Lazzeri A (2015) synergistic effects of nucleating agents and plasticizers on the crystallization behavior of poly(lactic acid). *Molecules* 20:1579–1593
- [27] Díez-Rodríguez TM, Blázquez-Blázquez E, Pérez E, Cerrada ML (2022) Influence of content in D isomer and incorporation of SBA-15 silica on the crystallization ability and mechanical properties in PLLA based materials. *Polymers* 14:1237
- [28] Watanabe R, Hagihara H, Sato H (2018) Structure–property relationships of polypropylene-based nanocomposites obtained by dispersing mesoporous silica into hydroxyl-functionalized polypropylene. Part 2: Matrix–filler interactions and pore filling of mesoporous silica characterized by evolved gas analysis. *Polym J* 50:1067–1077
- [29] Zhang J, Tashiro K, Tsuji H, Domb AJ (2008) Disorder-to-order phase transition and multiple melting behavior of poly(l-lactide) investigated by simultaneous measurements of WAXD and DSC. *Macromolecules* 41:1352–1357
- [30] Beltrán FR, de la Orden MU, Lorenzo V, Pérez E, Cerrada ML, Martínez-Urreaga J (2016) Water-induced structural changes in poly(lactic acid) and PLLA-clay nanocomposites. *Polymer* 107:211–222



- [31] Watanabe R, Hagihara H, Sato H (2018) Structure-property relationship of polypropylene-based nanocomposites by dispersing mesoporous silica in functionalized polypropylene containing hydroxyl groups. Part 1: toughness, stiffness and transparency. *Polym J* 50:1057–1065
- [32] Bento A, Lourenço JP, Fernandes A, Cerrada ML, Ribeiro MR (2013) Functionalization of mesoporous MCM-41 (nano)particles: preparation methodologies, role on catalytic features and dispersion within PE nanocomposites. *ChemCatChem* 5:966–976
- [33] Baiardo M, Frisoni G, Scandola M, Rimelen M, Lips D, Ruffieux K, Wintermantel E (2003) Thermal and mechanical properties of plasticized poly(L-lactic acid). *J Appl Polym Sci* 90:1731–1738
- [34] Yasuniwa M, Tsubakihara S, Sugimoto Y, Nakafuku C (2004) Thermal analysis of the double-melting behavior of poly (L-lactic acid). *J Polym Sci B: Polym Phys* 42:25–32
- [35] Ling X, Spruiell JE (2006) Analysis of the complex thermal behavior of poly (l-lactic acid) film. I. Samples crystallized from the glassy state. *J Polym Sci B: Polym Phys* 44:3200–3214
- [36] Di Lorenzo ML (2006) Calorimetric analysis of the multiple melting behavior of poly (L-lactic acid). *J Appl Polym Sci* 100:3145–3151
- [37] Pan P, Kai W, Zhu B, Dong T, Inoue Y (2007) Polymorphic crystallization and multiple melting behavior of poly(L-lactide): molecular weight dependence. *Macromolecules* 40:6898–6905
- [38] Kawai T, Rahman N, Matsuba G, Nishida K, Kanaya T, Nakano M, Okamoto H, Kawada J, Usuki A, Honma N, Nakajima K, Matsuda M (2007) Crystallization and melting behavior of poly (L-lactic acid). *Macromolecules* 40:9463–9469
- [39] Mandelkern L (1964) In *crystallization of polymers*. McGraw-Hill, New York, USA
- [40] Hoffman JD, Davis GT, Lauritzen JI (1976) In *treatise of solid state chemistry*. Plenum, New York, USA
- [41] Hoffman JD, Weeks JJ (1962) Melting process and the equilibrium melting temperature of polychlorotrifluoroethylene. *J Res Natl Bur Stand Sect A Phys Chem* 66(1):13
- [42] Marano S, Laudadio E, Minelli C, Stipa P (2022) Tailoring the barrier properties of PLA: a state-of-the-art review for food packaging applications. *Polymers* 14:1626
- [43] Molinari G, Aliotta L, Gemmi M, Lazzeri A, Righetti MC (2024) Constrained amorphous interphase in plasticized poly(lactic acid): composition and tensile elastic modulus estimation. *Polym Testing* 131:108325
- [44] Zhang J, Duan Y, Sato H, Tsuji H, Noda I, Yan S, Ozaki Y (2005) Crystal modifications and thermal behavior of poly(l-lactic acid) revealed by infrared spectroscopy. *Macromolecules* 38:8012–8021
- [45] Kister G, Cassanas G, Vert M (1998) Effects of morphology, conformation and configuration on the IR and Raman spectra of various poly(lactic acid)s. *Polymer* 39:267–273
- [46] Pan PJ, Zhu B, Dong T, Koji Y, Schimizu T, Tansho M, Inoue Y (2008) Conformational and microstructural characteristics of poly(L-lactide) during glass transition and physical aging. *J Chem Phys* 129:184902

**Publisher's Note** Springer Nature remains neutral with regard to jurisdictional claims in published maps and institutional affiliations.